Non-singlet spin structure function in the valon model and low-x-scaling behavior of $g_1^{\rm NS}$ and g_1^p

Fatemeh Taghavi-Shahri*
School of Particles and Accelerators, Institute for Research in Fundamental Sciences (IPM), Post Office Box 19395-5531, Tehran, Iran

Firooz Arash
Physics Department, Tafresh University, Tafresh, Iran
(Received 3 April 2010; published 15 September 2010)

A next-to-leading order QCD calculation of non-singlet spin structure function, $g_1^{\rm NS}$ is presented within the valon representation of hadrons. In the valon model, it is assumed that a nucleon is composed of three dressed valence quarks: the valons. Each valon has its own internal structure, the valence quark with its associated sea quarks and gluons. The results are in good agreement with all available data from SMC, E143, HERMES, and with the newly released data from COMPASS experiments. It appears that the small-x tail of $g_1^{\rm NS}$ can be described by a single Regge-type exchange. The relevant parameter of this exchange is given. Finally we show that the polarized proton structure function has a scaling behavior at small x. The relevant parameters of this behavior are given, too.

DOI: 10.1103/PhysRevC.82.035205 PACS number(s): 13.60.Hb, 12.38.Bx, 12.39.−x, 14.65.Bt

I. INTRODUCTION

Deep inelastic scattering (DIS) of leptons from the nucleon has served as an important tool for the investigation of the nucleon substructure and is one of the key areas for testing the quantum chromodynamics (QCD). Spin is a fundamental property of the nucleon and the spin structure of the nucleon has been the subject of heated debates over the past 20 years. The key question is how the spin of the nucleon is distributed among its constituent partons. That is, the determination and understanding of the shape of quarks and gluon spin distribution functions, $\delta q_f(x, Q^2)$, have became an important issue.

We utilized the valon model [1] to study the polarized nucleon structure. In the valon model, it is assumed that a nucleon is composed of three dressed valence quarks: the valons. Each valon has its own internal structure, the valence quark with its associated sea quarks and gluons which can be probed at high enough Q^2. At low Q^2, a valon behaves as a valence quark. The valons play a role in scattering problems as the constituents do in bound-state problems. It is assumed that the valons stand at a level in between hadrons and partons and that the valon distributions are independent of the probe or Q^2. In this representation a valon is viewed as a cluster of its own partons. The evolution of the parton distributions in a hadron is effected through the evolution of the valon structure, as the higher resolution of a probe reveals the parton content of the valon. This model has yielded excellent results for unpolarized structure functions [1–6]. It has also been applied to the polarized nucleon structure function [7,8] with interesting results.

In this paper we concentrate on the non-singlet part of the polarized nucleon structure function because of its simplicity and thus its transparency. In addition, there are more accurate data which are extended to a fairly small-x region: $x < 0.01$. That makes the comparison with theory more meaningful. Recently COMPASS Collaboration released data on $g_1^{\rm NS}$ to test the Bjorken sum rule with more accuracy [9]. Therefore, we have further attempted to show the application of using this model for studying the nucleon structure functions.

This paper is organized as follows. In Sec. II a brief general outline is presented on the calculation of the polarized nucleon structure function in the valon model. Then we calculate the non-singlet spin structure function in Sec. III. Finally, Sec. IV is devoted to study the Regge behavior of $g_1^{\rm NS}$ at small x and scaling behavior of g_1^p. Then, we will finish with conclusions.

II. VALON MODEL AND POLARIZED HADRON STRUCTURE FUNCTION

The connection between the bound-state problem at the hadronic scale that occurs only at low Q^2 and deep inelastic scattering at high Q^2 can be investigated by introducing the valons. Each valon is a dressed valence quark (i.e., each being a valence quark with its associated sea quarks and gluons which can be resolved only at high Q^2). At low Q^2 the valon behaves as a CQ because its internal structure cannot be resolved. Thus the valon distribution in a hadron is the wave-function square of the CQs, whose structure functions are described by PQCD at high Q^2 [2].

The valon model is essentially a two components model. See Fig. 1 for a schematic of the valon model. In this framework, the structure function $F_2(x, Q^2)$ of a hadron is a convolution of the valon distribution $G^h_{\rm valon}(y)$ and the structure function of the valon, $F_2^{\rm valon}(z, Q^2)$,

$$F_2^h(x, Q^2) = \sum_{\rm valon} \int_x^1 dy G^h_{\rm valon}(y) F_2^{\rm valon}\left(\frac{x}{y}, Q^2\right). \quad (1)$$

*f_taghavi@ipm.ir

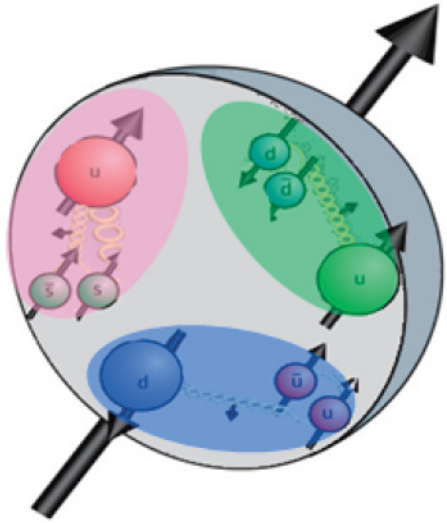

FIG. 1. (Color online) The schematic picture of the valon model.

In a similar way the parton distribution functions in a hadron can be obtained by

$$q(x, Q^2) = \sum_{\text{valon}} \int_x^1 dy G^h_{\text{valon}}(y) q^{\text{valon}}\left(\frac{x}{y}, Q^2\right), \quad (2)$$

where $G^h_{\text{valon}}(y)$ is the valon distribution inside the hadron. It means the probability of finding a valon with momentum fraction of y in the hadron. The description of the $G^h_{\text{valon}}(y)$ is given in [1,2].

In the polarized case, the helicity distributions of various partons in a hadron in the framework of this model are given by

$$\delta q^h_i(x, Q^2) = \sum \int_x^1 \frac{dy}{y} \delta G^h_{\text{valon}}(y) \delta q_i^{\text{valon}}\left(\frac{x}{y}, Q^2\right), \quad (3)$$

where $\delta G^h_{\text{valon}}(y)$ is the helicity distribution of the valon in the hosting hadron (the probability of finding the polarized valon inside the polarized hadron). It is related to unpolarized valon distribution by

$$\begin{aligned}\delta G_j(y) &= \delta F_j(y) G_j(y) \\ &= N_j y^{\alpha_j}(1-y)^{\beta_j}(1 + a_j y^{0.5} + b_j y + c_j y^{1.5} + d_j y^2).\end{aligned} \quad (4)$$

$G_j(y)$ are the unpolarized valon distributions, where j refers to U- and D-type valons. [Regrettably, Eq. (4) was erroneous in Ref. [7] in which $\delta G_j(y)$ was replaced by $\delta F_j(y)$.] Polarized valon distributions are determined by a phenomenological argument for a number of hadrons [7,8]. We summarized the parameters for Eq. (2.4) in Table I.

TABLE I. Numerical values of the parameters in Eq. (4).

Valon (j)	N_j	α_j	β_j	a_j	b_j	c_j	d_j
U	3.44	0.33	3.58	−2.47	5.07	−1.859	2.780
D	−0.568	−0.374	4.142	−2.844	11.695	−10.096	14.47

We come back to Eq. (3): $\delta q_i^{\text{valon}}(z = x/y, Q^2)$ is the polarized parton distribution in the valon. Polarized parton distributions inside the valon are evaluated according to the Dokshitzer-Gribov-Lipatov-Altarelli-Parisi (DGLAP) evolution equation subject to physically sensible initial conditions.

$$\begin{aligned}\delta q^{\text{NS}\pm}(n, Q^2) = &\left[1 + \frac{\alpha_s(Q^2) - \alpha_s(Q_0^2)}{2\pi}\left(\frac{-2}{\beta_0}\right)\right. \\ &\left.\times\left(\delta \mathbf{P}^{(1)n}_{\text{NS}\pm} - \frac{\beta_1}{2\beta_0}\delta \mathbf{P}^{(0)n}_{qq}\right)\right] \\ &\times \mathbf{L}^{-(\frac{2}{\beta_0})} \delta P^{(0)n}_{qq} \delta q^{NS\pm}(n, Q_0^2),\end{aligned} \quad (5)$$

$$\begin{aligned}\begin{pmatrix}\delta q^S(n, Q^2) \\ \delta g(n, Q^2)\end{pmatrix} = &\left(\mathbf{L}^{-(\frac{2}{\beta_0})\delta \hat{P}^{(0)n}} + \frac{\alpha_s(Q^2)}{2\pi}\hat{\mathbf{U}}\mathbf{L}^{-(\frac{2}{\beta_0})\delta \hat{P}^{(0)n}}\right. \\ &\left.-\frac{\alpha_s(Q_0^2)}{2\pi} L^{-(\frac{2}{\beta_0})\delta \hat{P}^{(0)n}} \hat{\mathbf{U}}\right)\begin{pmatrix}\delta q^S(n, Q_0^2) \\ \delta g(n, Q_0^2)\end{pmatrix}.\end{aligned} \quad (6)$$

The detail of Eqs. (5) and (6) are given in [15]. As presented in [7] and [8], we have calculated the polarized nucleon structure function in the valon model. We have worked in the $\overline{MS}$ scheme with $\Lambda_{\text{QCD}} = 0.22$ GeV and $Q_0^2 = 0.283$ GeV^2. The initial motivation for this value of Q_0^2 comes from the phenomenological consideration that requires us to choose the initial input densities as $\delta(z-1)$ at Q_0^2. The valon structure function has the property that it becomes $\delta(z-1)$ as Q^2 is extrapolated to Q_0^2 (beyond the region of validity). This mathematical boundary condition means that the internal structure of the valon cannot be resolved at Q_0^2 in next to leading order (NLO) approximation. It also means that at the initial scale of Q_0^2, the nucleon can be considered as a bound state of three valence quarks that carry all the momentum and the spin of the nucleon. As Q^2 is increased other partons can be resolved at the nucleon. It is also interesting to note that this value of Q^2 is very close to the transition region reported by the CLAS Collaboration. Measurement of the first moment of the proton structure function at CLAS shows that there is a transition region around $Q^2 = 0.3$ GeV^2 [10]. Therefore the initial input densities to solve the DGLAP equations inside the valon are

$$\delta q^{NS}(z, Q_0^2) = \delta q^S(z, Q_0^2) = \delta(z-1), \quad (7)$$

$$\delta g(z, Q_0^2) = 0. \quad (8)$$

Thus their moments are

$$\delta q^{\text{NS}}(n, Q_0^2) = \delta q^S(n, Q_0^2) = \int_0^1 z^{n-1}\delta(z-1)dz = 1, \quad (9)$$

$$\delta g(n, Q_0^2) = 0. \quad (10)$$

In the valon model, the hadron structure is obtained by the convolution of the valon structure and its distribution inside the hadron. Having specified the various components that contribute to the spin of a valon, we now turn to the

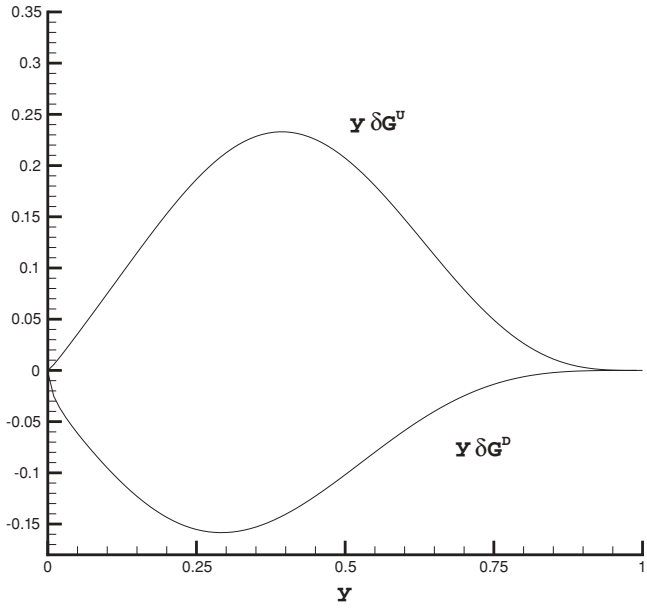

FIG. 2. Polarized valon distributions for U and D valons inside the proton.

polarized hadron structure, which is obtained by a convolution integral as follows:

$$g_1^h(x, Q^2) = \sum_{\text{valon}} \int_x^1 \frac{dy}{y} \delta G^h_{\text{valon}}(y) g_1^{\text{valon}}\left(\frac{x}{y}, Q^2\right). \qquad (11)$$

The valon structure is generated by perturbative dressing in QCD. In such processes with massless quarks, helicity is conserved and, therefore, the hard gluons cannot induce sea quark polarization perturbatively. According to this description, it turns out that sea polarization is consistent with zero [7]. This finding is supported by the HERMES experiment and by released data from the COMPASS experiment [11–14]. Therefore we have no sea polarization in our model.

Using the initial conditions in Eqs. (9) and (10), the calculation of the polarized parton distribution functions (PPDFs) inside the valon follow from the standard DGLAP evolution equations. The algorithm for calculation of the PPDFs inside the proton can be decomposed in the following three steps:

(i) Calculating PPDFs in the valon by using the DGLAP equations.
(ii) With a phenomenological approach, one can find the helicity distributions for the valons, as in Fig. 2. These functions are Q^2 independent. Since we find the valon helicity distributions, one can use them to calculate the polarized nucleon structure up to $Q^2 = 10^7$ GeV^2.
(iii) By using the convolution integral [Eqs. (3) and (11)], one finds PPDFs in the nucleon and polarized structure function.

There is excellent agreement between the model predictions with the experimental data for spin structure functions. A sample is given in Fig. 3.

III. NON-SINGLET SPIN STRUCTURE FUNCTION

The non-singlet polarized parton distribution function is defined as $\Delta q^{\text{NS}}(x,t) = (\Delta u - \Delta d)(x,t)$, with $t = \ln \frac{Q^2}{\Lambda^2}$.

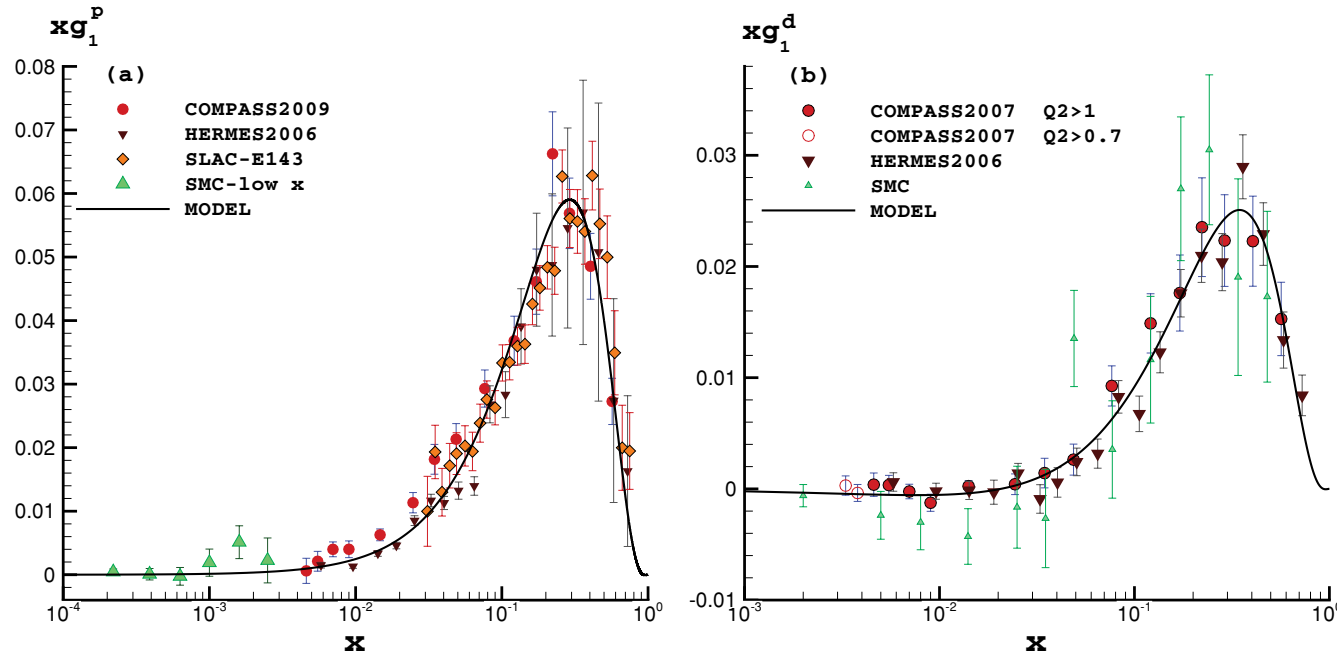

FIG. 3. (Color online) (a) Polarized proton structure function xg_1^p at $Q^2 = 5$ GeV^2 ($\frac{\chi^2}{N} = 1.7$). (b) Polarized deuteron structure function xg_1^d at $Q^2 = 3$ GeV^2 ($\frac{\chi^2}{N} = 1.33$). The results from model [7] are compared with the experimental data [9,11,13,16–18]. The data from Ref. [9] are newly released data from COMPASS.

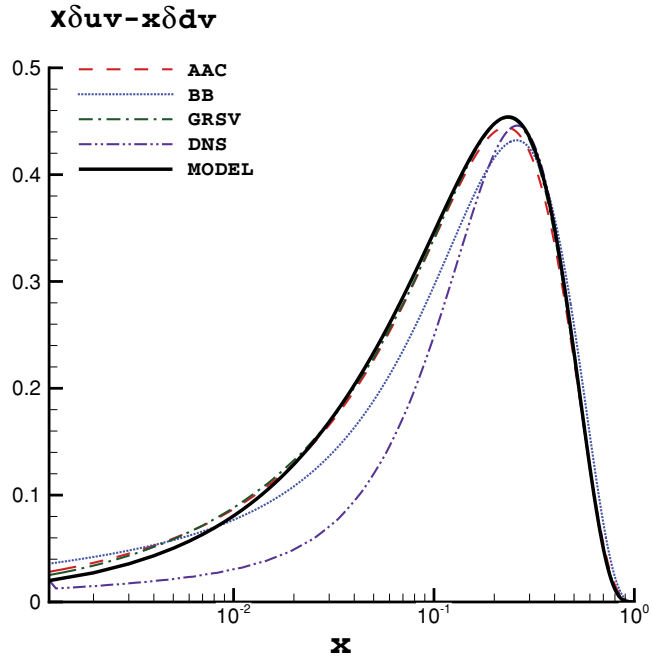

FIG. 4. (Color online) The non-singlet polarized parton distribution function in the valon model in comparison with other global fits [19–22].

The DGLAP equation for $\Delta q^{\rm NS}(x,t)$ is

$$\frac{d}{dt}\Delta q^{\rm NS} = \int_x^1 \frac{dy}{y} P\left(\frac{x}{y}\right) \Delta q^{\rm NS}(y,t), \qquad (12)$$

where $P(z = x/y)$ is the NLO spin-dependent splitting function [15]. As mentioned earlier, in our calculations $\Delta q_{\rm sea} \simeq 0$; therefore, $\Delta q^{\rm NS}$ becomes $(\Delta u_V - \Delta d_V)(x,t)$ which is shown in Fig. 4 in comparison with other global fits. The non-singlet spin structure function is defined as

$$g_1^{\rm NS} \equiv g_1^p - g_1^n = 2\left[g_1^p - g_1^d/(1 - 1.5\omega_D)\right], \qquad (13)$$

where $\omega_D = 0.058$ accounts for the D-state admixture in the deuteron wave function.

The $g_1^{\rm NS}$ data are consistent with the quark model and the perturbative QCD predictions in the valence region $x > 0.2$ [23].

In Fig. 5(a), the x dependence of $xg_1^{\rm NS}$ is shown in comparison with data from HERMES, E143, SMC, and also with the newly released data from COMPASS [9]. The results are in very good agreement with experimental data for the entire measured range of x. In Fig. 5(b) the evolution of the Bjorken integral, derived from Fig. 5(a), $\int_{x\min}^1 [\frac{1}{x}(xg_1^{\rm NS})]dx = \int_{x\min}^1 (g_1^{\rm NS})dx$ as a function of $x_{\min}$, is shown for the model compared with the recent HERMES and COMPASS Collaboration data [9,11]. Note that about 50% of the sum rule comes from x values below about 0.12 and that about 10–20 % comes from values of x less than about 0.01. It shows that $g_1^{\rm NS}$ receives a considerable contribution from the small-x region. Thus, it seems that investigation of the small-x region of the structure function is important. In the following section we will consider $g_1^{\rm NS}$ at this region. In Table II we compared the integral over different x ranges at different scales of Q^2, as determined from the valon model with the experimental results from COMPASS, HERMES, E143, E154, E155, SMC, and JLAB also with the recent results from NN Collaborations [9,10,16–18,24–27]. We have used data from JLAB for $Q^2 > 0.5$ GeV^2 to make sure that the nonperturbative effects are small.

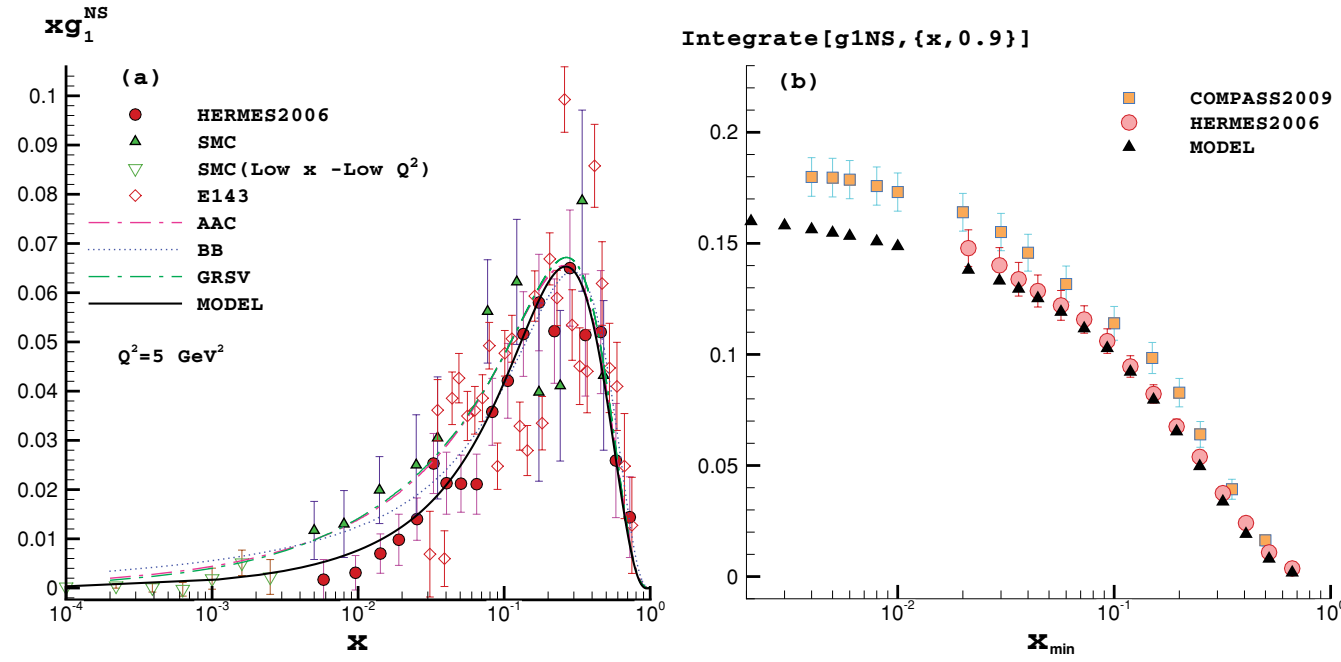

FIG. 5. (Color online) (a) $xg_1^{\rm NS}$ at $Q^2 = 5$ GeV^2 compared with the experimental data and the results from global fits [19–21] ($\frac{\chi^2}{N} = 1.25$). (b) The integral of $g_1^{\rm NS}$ over the range $0.02 < x < 0.9$ measured by HERMES and COMPASS Collaborations as a function of the low-x limit of integration, $x_{\min}$, evaluated at $Q^2 = 10$ GeV^2 in comparison with our results.

TABLE II. Comparison of the integral over different x ranges at different scales of Q^2, as determined from the valon model, with the experimental results from COMPASS, HERMES, E143, E154, E155, SMC, and JLAB also with the results from NN Collaborations.

Experiment	x range	Q^2	Γ_1^{NS}	This analysis
COMPASS	$0.004 < x < 0.7$	3	$0.175 \pm 0.009 \pm 0.015$	0.1421
HERMES	$0.021 < x < 0.9$	5	0.1479 ± 0.0169	0.1381
E143	$0.03 < x < 0.8$	2	0.149 ± 0.016	0.1276
E143	$0.03 < x < 0.8$	3	0.164 ± 0.023	0.1301
E143	$0.03 < x < 0.8$	5	0.141 ± 0.013	0.1327
E154	$0.03 < x < 0.8$	5	0.168 ± 0.010	0.1327
E155	$0.03 < x < 0.8$	5	0.176 ± 0.008	0.1327
SMC	$0 < x < 1$	10	0.198 ± 0.023	0.1626
SMC	$0 < x < 1$	5	$0.174 \pm 0.024 \pm 0.012$	0.1569
JLAB	$0.001 < x < 0.8$	0.592	$0.1027 \pm 0.0228 \pm 0.0052$	0.123
JLAB	$0.001 < x < 0.8$	0.707	$0.0945 \pm 0.0201 \pm 0.0151$	0.1298
JLAB	$0.001 < x < 0.8$	0.844	$0.1021 \pm 0.0193 \pm 0.0174$	0.134
JLAB	$0.001 < x < 0.8$	1.20	$0.1307 \pm 0.0192 \pm 0.0145$	0.1323
JLAB	$0.001 < x < 0.8$	1.44	$0.1522 \pm 0.0186 \pm 0.0089$	0.1433
JLAB	$0.001 < x < 0.8$	1.71	$0.1605 \pm 0.0182 \pm 0.0069$	0.1318
JLAB	$0.001 < x < 0.8$	2.05	$0.1678 \pm 0.0177 \pm 0.0056$	0.1475
JLAB	$0.001 < x < 0.8$	2.44	$0.1666 \pm 0.0167 \pm 0.0045$	0.1492
JLAB	$0.001 < x < 0.8$	2.92	$0.1789 \pm 0.0106 \pm 0.0035$	0.1511
NN Collaboration	$0.021 < x < 0.9$	5	0.1315 ± 0.0144	0.1381

IV. REGGE BEHAVIOR OF g_1^{NS} AND FULL g_1^p AT SMALL x

In all the results from experimental data for unpolarized and polarized structure functions, it is seen that these structure functions increase when x decreases and Q^2 increases for fixed values of x and Q^2, respectively. The small-x behavior of spin-dependent structure functions reflects the high-energy behavior of the polarized virtual Compton scattering total cross section with increasing total CM energy squared W^2 since $W^2 = Q^2(\frac{1}{x} - 1)$. When $W^2 \gg Q^2$, x is small and $W^2 \approx Q^2/x$ and then at this region the structure functions have scaling behavior. This is, by definition, the Regge limit and so the Regge pole exchange picture is therefore quite appropriate for the theoretical description of this behavior [28]. The small-x or high-energy behavior of the spin structure function is an important issue for the extrapolation of data needed to test spin sum rules for the first moment of g_1. The small-x measurements, besides reducing the error on the first moment, would provide valuable information about Regge and QCD dynamics at small x where the shape of g_1 is particularly sensitive to the different theoretical input.

In the case of the unpolarized structure function F_2, it is believed that a Regge trajectory combined with a soft and a hard Pomeron can accurately represent the experimental data [29]. It is interesting to investigate this issue in the polarized case.

The Regge pole model gives the following small-x behavior of the structure functions $g_1^i(x, Q^2)$ [28]

$$g_1^i(x, Q^2) = \gamma_i(Q^2)x^{-\alpha_i}, \tag{14}$$

where $g_1^i(x, Q^2)$ denote either a singlet $[g_1^s(x, Q^2) = g_1^p(x, Q^2) + g_1^n(x, Q^2)]$ or non-singlet $[g_1^{NS}(x, Q^2) = g_1^p(x, Q^2) - g_1^n(x, Q^2)]$ combination of structure functions. Therefore we expect to describe the small-x behavior of g_1^{NS} and g_1^p structure functions with one and two Regge exponents, respectively. It appears that the present g_1^{NS} data for available small x in the interval $0.0001 < x < 0.01$ can be described with a single Regge-type exchange as

$$g_1^{NS} \equiv g_1^p - g_1^n \simeq Ax^{\alpha_{\text{Regge}}}. \tag{15}$$

The Regge intercept that governs the small-x physics has smooth Q^2 dependence, in which case one would see g_1^{NS} rising like x^α where $-0.5 \leqslant \alpha \leqslant 0$ also at low Q^2 and in the measured "small-x" region [30]. This value varies from -0.13 to -0.3 when Q^2 is moved from $Q^2 = 2$ GeV^2 to $Q^2 = 10$ GeV^2 in the valon model. According to the results of Ref. [31], asymptotic scaling of g_1^{NS} depends on one variable Q^2/x^2 only, instead of two variables x and Q^2 with the constant intercept equal to 0.42:

$$g_1^{NS} \simeq (Q^2/x^2)^{\Delta_{NS}/2} \simeq Q^{\Delta_{NS}}x^{-\Delta_{NS}}, \quad \Delta_{NS} = 0.42. \tag{16}$$

However, it is valid for a very small-x only. The applicability region of that analysis is $x \leqslant 10^{-6}$. Figure 6 shows the non-singlet spin structure function at $Q^2 = 5$ GeV^2 for the small-x region. In Fig. 7, we fit the non-singlet spin structure function at small x $(0.0001 < x < 0.01)$ and find the associated α_{Regge}:

$$g_1^{NS} = Ax^{\alpha_{\text{Regge}}}, \quad A = 0.173, \quad \alpha_{\text{Regge}} = -0.323. \tag{17}$$

A. Scaling behavior of g_1^p at small x

Having analyzed the small-x behavior of g_1^{NS}, it is interesting to see how g_1^p behaves as $x \to 0$. Because the valon model has very good agreement with existent small-x data, it is a good candidate to show the small-x behavior of g_1^p at small x. Actually the results for this scaling behavior should be compared with small-x data for g_1^p.

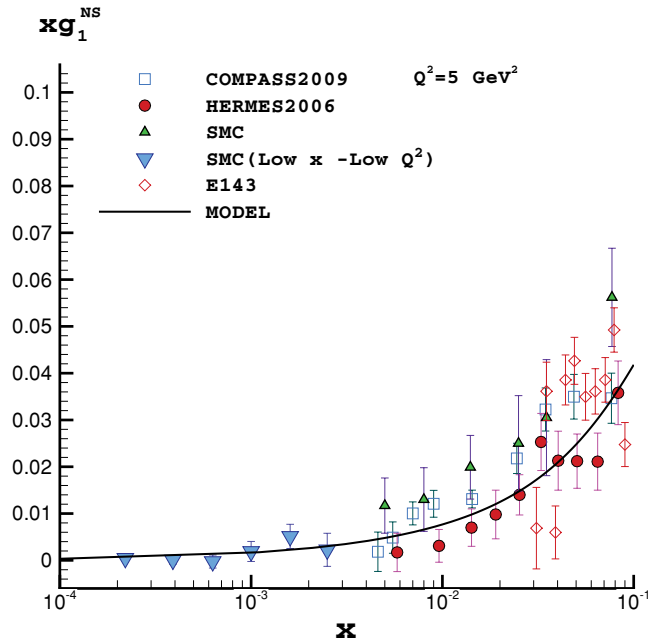

FIG. 6. (Color online) Small-x behavior of $xg_1^{\rm NS}$ at $Q^2 = 5$ GeV^2 calculated by using the valon model in comparison with the experimental data.

We show that the polarized proton structure function has this scaling behavior for $1.2 < Q^2(\text{GeV}^2) < 100$ at small-x ($10^{-5} < x < 10^{-2}$),

$$g_1^p(x, Q^2) = \sum_{i=1}^{2} a_i f_i(Q^2) x^{\varepsilon_i}, \tag{18}$$

where a_i and ε_i are constants and the functions $f_i(Q^2)$ have this simple general form,

$$f_2(Q^2) = \left(\frac{Q^4}{1+Q_0^4}\right)^{D_i}, \quad f_1(Q^2) = f_2(Q^2) g(Q^2), \tag{19}$$

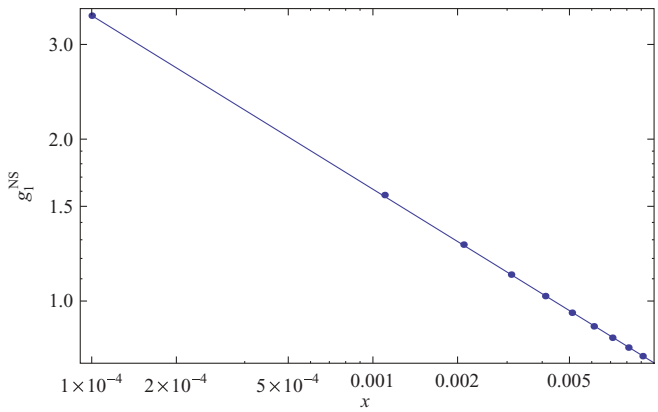

FIG. 7. (Color online) Small-x behavior of $g_1^{\rm NS}$ at $Q^2 = 5$ GeV^2 calculated by using the valon model and using the best fit to calculate the Regge exponent. Data points are from the model and the goodness of fit is $\chi^2 = 0.99$.

TABLE III. Global fit parameters obtained by fitting Eq. (18) with the data extracted from the valon model at small x.

Parameters	Values
ε_1	0.196
ε_2	0.094
a_1	0.0215
a_2	0.0513
D_1	0.759
D_2	0.434
g_0	17.538
g_1	−11.809
g_2	2.652
g_3	−0.200
Q_0	1.300
χ^2 (goodness of fit)	0.996

where

$$g(Q^2) = g_0 + g_1 \log(Q^2) + g_2 \log(Q^2)^2 + g_3 \log(Q^2)^3. \tag{20}$$

The results for parametrization of g_1^p are summarized in Table III. (We should note that if we try to do a fit with only one Regge exponent and only with the first term in Eq. (18), we give a fit with $\chi^2 = 0.99$. So, it is clear that we can describe the polarized proton structure function with two exponents, $\chi^2 = 0.996$, which is better than one exponent.)

In Fig. 8 we show the small-x behavior of xg_1^p at $Q^2 = 5$ GeV^2 calculated by using the valon model and using the

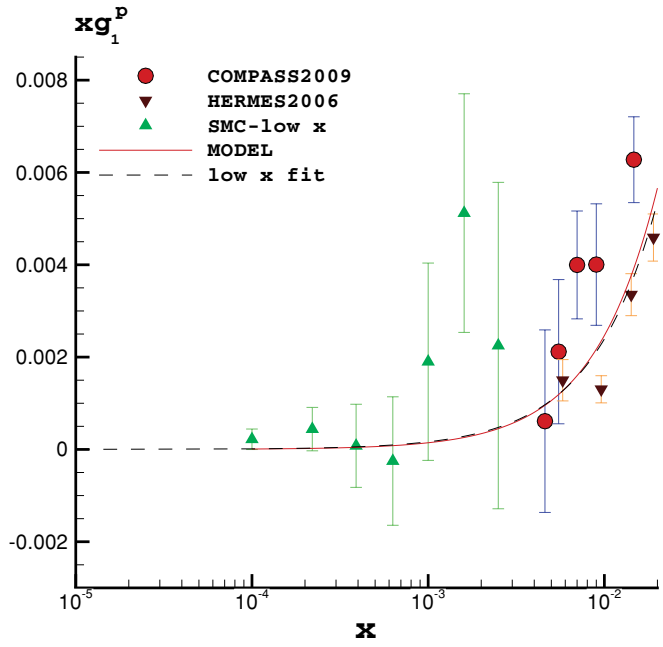

FIG. 8. (Color online) Small-x behavior of xg_1^p at $Q^2 = 5$ GeV^2 calculated by using the valon model and using the best fit to calculate the scaling exponents at small x. The experimental data selected for various Q^2 at the small-x region.

best fit to calculate the scaling exponents, ε_i. As a result, we concluded that only by using two scaling exponents can we describe the small-x behavior of $g_1^p(x, Q^2)$ well. This behavior has also been seen in the small-x tail of the $F_2^p(x, Q^2)$ structure function [28]. The question has been raised [32,33] whether the observed rise on $g_1^{\rm NS}(x, Q^2)$ follows from a one or two Pomeron exchange (a polarized analog of the one or two Pomerons question). However, after looking at $g_1^p(x, Q^2)$, it indeed requires two Pomerons!

V. CONCLUSION

In this paper we calculated the non-singlet spin structure function, $g_1^{\rm NS}$, of the nucleon in the valon model. The results of these calculations are in excellent agreement with all experimental data for the entire measured range of x. We also study the small-x behavior of non-singlet spin structure function and the Regge behavior of $g_1^{\rm NS}$ to calculate the Regge exponent, $\alpha_{\rm Regge}$. Finally, we studied the scaling behavior of g_1^p at small x. We conclude that only by using two scaling exponents can we describe the small-x behavior of g_1^p well. This is very similar to the existence of two soft and hard Pomerons to describe the small-x behavior of $F_2(x, Q^2)$ in the unpolarized case. It is shown that the valon model can predict the polarized nucleon structure functions for the entire measured x range very well. The validity range for using the valon model is $0.5 < Q^2\ ({\rm GeV}^2) < 10^7$ and $10^{-6} < x < 1$. In this model sea quarks polarization is consistent with zero (the finding that was confirmed by very recent experiments at HERMES and COMPASS), so the polarized hadron structure functions can build only by the polarized valence and gluon distribution by finding only one type of polarized valon distribution for each kind of valons. Between $0.3 < Q^2\ ({\rm GeV}^2) < 0.5$ we should consider other effects, such as a combination of resonance physics and vector-meson dominance that are important at low Q^2. Chiral perturbation theory may describe the behavior of polarized nucleon structure close to threshold. These issues will be considered in our future work to improve our model.

ACKNOWLEDGMENTS

We would like to thank Professor G. Altarelli for his careful reading of the manuscript and for the productive discussions. F. Taghvi-Shahri thanks A. Korzenev for his help and also thanks Dr. M. Khakzad for reading the manuscript.

[1] R. C. Hwa, Phys. Rev. D **22**, 759 (1980).
[2] R. C. Hwa, arXiv:0904.2159v1 [hep-ph].
[3] R. C. Hwa and C. B. Yang, Phys. Rev. C **66**, 025205 (2002).
[4] F. Arash and A. N. Khorramian, Phys. Rev. C **67**, 045201 (2003).
[5] F. Arash, Phys. Lett. B **557**, 38 (2003).
[6] F. Arash, Phys. Rev. D **69**, 054024 (2004).
[7] F. Arash and F. Taghavi-Shahri, J. High Energy Phys. 07 (2007) 071.
[8] F. Arash and F. Taghavi-Shahri, Phys. Lett. B **668**, 193 (2008).
[9] M. G. Alekseev (COMPASS Collaboration), Phys. Lett. B **690**, 466 (2010).
[10] R. Fatemi *et al.* (CLAS Collaboration), Phys. Rev. Lett. **91**, 222002 (2003).
[11] A. Airapetian *et al.* (HERMES Collaboration), Phys. Rev. D **75**, 012007 (2007).
[12] A. Airapetian *et al.* (HERMES Collaboration), Phys. Lett. B **666**, 446 (2008).
[13] M. G. Alekseev (COMPASS Collaboration), Phys. Lett. B **660**, 458 (2008); V. Yv. Alexakhin *et al.*, *ibid.* **647**, 8 (2007).
[14] M. Alekseev *et al.* (COMPASS Collaboration), Phys. Lett. B **680**, 217 (2009).
[15] B. Lampe and E. Reya, Phys. Rep. **332**, 1 (2000).
[16] B. Adeva *et al.* (SMC Collaboration), Phys. Rev. D **58**, 112001 (1998).
[17] B. Adeva *et al.* (SMC Collaboration), Phys. Rev. D **60**, 072004 (1999).
[18] K. Abe *et al.* (E143 Collaboration), Phys. Rev. Lett. **75**, 25 (1995); Phys. Rev. D **58**, 112003 (1998).
[19] Y. Goto *et al.* (Asymmetry Analysis Collaboration), Phys. Rev. D **62**, 034017 (2000); **69**, 054021 (2004).
[20] J. Blumlein and H. Bottcher, Nucl. Phys. B **636**, 225 (2002).
[21] M. Gluck, E. Reya, M. Stratmann, and W. Vogelsang, Phys. Rev. D **63**, 094005 (2001).
[22] D. de Florian, G. A. Navarro, and R. Sasso, Phys. Rev. D **71**, 094018 (2005).
[23] S. D. Bass, Eur. Phys. J. A **5**, 17 (1999).
[24] K. Abe *et al.* (E154 Collaboration), Phys. Lett. B **405**, 180 (1997).
[25] P. L. Anthony *et al.* (E155 Collaboration), Phys. Lett. B **493**, 19 (2000).
[26] A. Deur *et al.*, Phys. Rev. D **78**, 032001 (2008).
[27] L. Del Debbio, A. Guffanti, and A. Piccione, J. High Energy Phys. 11 (2009) 060.
[28] J. Kwiecinski and B. Ziaja, Phys. Rev. D **60**, 054004 (1999).
[29] A. Donachie and P. V. Landshoff, Phys. Lett. B **595**, 393 (2004); Acta Phys. Pol. B **34**, 2989 (2003); Phys. Lett. B **533**, 277 (2002).
[30] J. Ellis and M. Karliner, Phys. Lett. B **213**, 73 (1988).
[31] B. I. Ermolaev, M. Greco, and S. I. Troyan, Riv. Nuovo Cim. **33** 57 (2010).
[32] S. D. Bass, Mod. Phys. Lett. A **22**, 1005 (2007).
[33] S. D. Bass, *The Spin Structure of the Proton* (World Scientific, Singapore, 2007), p. 212.